SCIENCE CHINA
Mathematics

• ARTICLES •

https://doi.org/10.1007/s11425-024-2337-3

Higher-order energy-decreasing exponential time differencing Runge-Kutta methods for gradient flows

Zhaohui Fu[1], Jie Shen[2,*] & Jiang Yang[3,4]

[1]*Department of Mathematics, National University of Singapore, Singapore* 119076*, Singapore;*
[2]*School of Mathematical Science, Eastern Institute of Technology, Ningbo* 315200*, China;*
[3]*Department of Mathematics, Southern University of Science and Technology, Shenzhen* 518055*, China;*
[4]*SUSTech International Center for Mathematics & National Center for Applied Mathematics Shenzhen (NCAMS), Southern University of Science and Technology, Shenzhen* 518055*, China*

Email: fuzhmath@gmail.com, jshen@eitech.edu.cn, yangj7@sustech.edu.cn

Received May 29, 2024; accepted September 30, 2024; published online November 22, 2024

Abstract In this paper, we develop a general framework for constructing higher-order, unconditionally energy-decreasing exponential time differencing Runge-Kutta (ETDRK) methods applicable to a range of gradient flows. Specifically, we identify conditions sufficient for ETDRK schemes to maintain the original energy dissipation. Our analysis reveals that the widely-employed third- and fourth-order ETDRK schemes fail to meet these conditions. To address this, we introduce new third-order ETDRK schemes, designed with appropriate stabilization, which satisfy these conditions and thus guarantee the unconditional energy decay property. We conduct extensive numerical experiments with these new schemes to verify their accuracy, stability, behavior under large time steps, long-term evolution, and adaptive time-stepping strategy across various gradient flows. This study offers the first framework to examine the unconditional energy stability of high-order ETDRK methods, and we are optimistic that our framework will enable the development of ETDRK schemes beyond the third order that are unconditionally energy stable.

Keywords exponential time differencing Runge-Kutta method, energy stability, gradient flows, phase-field models

MSC(2020) 65M12, 35K20, 35K35, 35K55

Citation: Fu Z H, Shen J, Yang J. Higher-order energy-decreasing exponential time differencing Runge-Kutta methods for gradient flows. Sci China Math, 2024, 67, https://doi.org/10.1007/s11425-024-2337-3

1 Introduction

We consider a class of gradient flows written in the following general form:

$$u_t = G(\mathcal{L}u + f(u)), \quad (x,t) \in \Omega \times [0,T], \tag{1.1}$$

where Ω is a bounded domain in $\mathbb{R}^d$ $(d = 1,2,3)$, T is a finite time, G is a nonpositive operator, and $\mathcal{L}$ is a positive definite operator. The above system is energy dissipative with the corresponding energy functional

$$E(u) = \int_\Omega \left(\frac{1}{2}|\mathcal{L}_{1/2}u|^2 + F(u)\right)dx, \tag{1.2}$$

* Corresponding author

where F satisfies that $F' = f$. This general form covers a wide range of gradient flows, such as the Allen-Cahn equation [2], the Cahn-Hilliard equation, and the thin film model without slope selection also known as the molecular beam epitaxy (MBE) model, the phase-field crystal models, etc.

Since these gradient flows involve strong nonlinearities and often high-order derivatives, it is difficult to design an efficient time discretization scheme which is able to accurately approximate their dynamics and steady states. In particular, it is challenging for numerical schemes to guarantee the energy decay which is intrinsic to all of these models. Ample numerical evidence indicates that non-physical oscillations may occur when the energy stability is violated. Furthermore, the establishment of unconditional energy stability enables the creation of more efficient algorithmic designs, including the development of adaptive time-stepping strategies, where the selection of time steps is solely governed by considerations of accuracy.

There have been a large number of studies concerning energy-stable schemes for gradient flows (see, e.g., [11,12,15,19,21,24,27,28,33,34,36,38] and the references therein). In particular, the convex splitting technique (see [31, 35]) is useful to preserve unconditional energy stability, but it leads to a nonlinear scheme and is not easy to extend to more general cases. The invariant energy quadratization (IEQ) method (see, e.g., [40, 41]) and the scalar auxiliary variable (SAV) method (see [6, 32]) lead to linear schemes that can preserve different structures for a wide class of gradient flows. In particular, there have been a large number of works based on SAV methods, including SAV-BDF schemes (see [5,20]) and SAV-RK schemes (see [1, 37]). However, the energy stability achieved by the IEQ or SAV methods is based on a modified energy, not the original energy. [13] also offers a framework introducing high-order implicit-explicit Runge-Kutta schemes for (1.1) which unconditionally decreases energy with respect to the original energy.

On the other hand, exponential time differencing Runge-Kutta (ETDRK) schemes offer many advantages over multistep methods. In this paper, we consider ETDRK methods for (1.1). The key idea of ETDRK schemes is to apply Duhamel's principle

$$u(x,t) = \mathrm{e}^{G\mathcal{L}(t-t_0)}u(x,t_0) - \mathrm{e}^{G\mathcal{L}(t-t_0)}\int_{t_0}^{t}\mathrm{e}^{-G\mathcal{L}(s-t_0)}Gf(u(x,s))ds \tag{1.3}$$

and approximate the implicit integral which contains the unknown $f(u(x,s))$ with an explicit RK method. The concept of exponential integrators has a long-standing history, tracing its origins back to the 1960s. There has been much literature related to using such methods to solve stiff problems, semilinear parabolic problems or gradient flows (see [7,8,10,14,17]). However, ETDRK schemes are usually not energy stable. It has been shown in [8,9] that some first-order ETDRK schemes can be energy stable. More recently, it is shown in [14] that a second-order ETDRK method with proper stabilization is unconditionally energy stable. A concrete third-order ETDRK scheme (see [3]) also provides a high-order solution for gradient flows. However, the question of whether general high-order ETDRK can maintain the energy dissipation property remains an open problem.

This paper aims to introduce a comprehensive framework for developing unconditionally energy-stable ETDRK schemes tailored for various gradient flows. We have formulated a series of criteria for ensuring the unconditional energy stability of ETDRK schemes of arbitrary order. Our investigations reveal that the widely-employed third- and fourth-order ETDRK methods fall short of meeting these criteria. In response, we have designed innovative third-order ETDRK schemes that adhere to these standards, thereby achieving unconditional energy stability. To our knowledge, this work pioneers the establishment of sufficient conditions for high-order ETDRK methods to attain unconditional energy stability. We are optimistic that this foundational framework will pave the way for the creation of advanced ETDRK schemes surpassing the third order in terms of unconditional energy stability.

The rest of this paper is organized as follows. In Section 2, we present some background knowledge, and then state and prove our main theorem. In Section 3, we apply the main theorem to various known ETDRK schemes and determine whether they are unconditionally energy-stable; in particular, we show that the commonly used third- and fourth-order ETDRK schemes do not satisfy these conditions, and we construct new third-order ETDRK schemes that satisfy these conditions and thus are unconditional energy stable. In Section 4, we present ample numerical experiments to validate our new third-order

schemes and study how large time steps affect the solutions, and how different time steps and stabilizers influence the energy evolution. We also present an example with adaptive time stepping to show the application of this scheme. Some concluding remarks are given in Section 5.

2 Energy decreasing ETDRK methods for gradient flows

In this section, we first introduce some basic knowledge of gradient flows, phase field models, convex splitting, and the ETDRK methods. Then we prove our main theorem, i.e., arbitrary ETDRK schemes are unconditionally energy stable as long as the conditions are satisfied.

2.1 Phase-field models

We consider the general form of gradient flows in a Hilbert space $\mathcal{H}$:

$$u_t = G(\mathcal{L}u + f(u)), \quad (x,t) \in \Omega \times [0,T], \tag{2.1}$$

where G is a nonpositive operator, $\mathcal{L}$ is a positive definite operator, and $f(u) = F'(u)$, where $F(u)$ is a nonlinear functional. In the following text, we denote the inner product by $(\cdot,\cdot)$. Taking the inner product of (2.1) with $\mathcal{L}u + f(u)$, we find the energy dissipation law

$$\frac{d}{dt}E(u) = (G(\mathcal{L}u + f(u)), \mathcal{L}u + f(u)) \leqslant 0, \tag{2.2}$$

where the free energy $E(u)$ is given by

$$E(u) = \int_\Omega \left(\frac{1}{2}(\mathcal{L}u, u) + F(u)\right)dx. \tag{2.3}$$

Some typical examples are provided below:

- the Allen-Cahn equation, $G = -I$, $\mathcal{L} = -\epsilon^2\Delta$, $f(u) = u^3 - u$, and $F(u) = \frac{1}{4}(u^2-1)^2$;
- the Cahn-Hilliard equation, $G = \Delta$, $\mathcal{L} = -\epsilon^2\Delta$, $f(u) = u^3 - u$, and $F(u) = \frac{1}{4}(u^2-1)^2$;
- the MBE model without slope selection, $G = -I$, $\mathcal{L} = -\epsilon^2\Delta^2$ but $f(u)$ should be replaced by

$$f(\nabla u) = -\nabla \cdot \left(\frac{\nabla u}{1 + |\nabla u|^2}\right),$$

and correspondingly, $F(\nabla u) = -\frac{1}{2}\ln(|\nabla u|^2 + 1)$;

- the phase field crystal equation, $G = \Delta$, $\mathcal{L} = (\Delta + 1)^2$, $f(u) = u^3 - \epsilon u$, and $F(u) = \frac{1}{4}(u^2 - \epsilon)^2$.

We assume that f is a Lipschitz continuous function with the Lipschitz constant C_L, i.e., we have

$$\|f(u) - f(v)\| \leqslant C_L\|u - v\|, \quad \forall\, u, v \in \mathcal{H}. \tag{2.4}$$

For the MBE model, the functions F and f depend only on ∇u, which is different from other examples. The Lipschitz condition is satisfied in the sense

$$\|\partial^2_{\nabla u} F(\nabla u)\|_2 \leqslant 1, \tag{2.5}$$

which also bounds the growth of the nonlinear term.

Notice that for the Cahn-Hilliard equation and the phase field crystal model, $f(u)$ does not naturally satisfy the Lipschitz assumption on nonlinearity, but we can truncate $f(u)$ to quadratic growth as in [14,34] so as to satisfy the Lipschitz assumption. In practice such a modification never affects anything because of the boundedness of their solutions (see [25, 26]), which offer solid analysis without Lipschitz assumptions.

Consider the natural splitting of the energy $E(u) = E_l - E_n$ with

$$\begin{aligned} E_l(u) &= \int_\Omega \left(\frac{1}{2}|\mathcal{L}_{1/2}u|^2 + \frac{\beta}{2}|u|^2\right)dx, \\ E_n(u) &= \int_\Omega \left(-F(u) + \frac{\beta}{2}|u|^2\right)dx. \end{aligned} \tag{2.6}$$

From this perspective, the gradient flow can thus be written as

$$u_t = G(Lu - g(u)), \tag{2.7}$$

where $L = \beta I + \mathcal{L}$ and $g = \beta I - f$ correspond to E_l and E_n, respectively. In the computation, Lu is treated implicitly and $g(u)$ is treated explicitly, which leads to linearly implicit schemes.

Here, β serves as a stabilization to enhance the dissipation of the linear part so as to bound the Lipschitz growing nonlinear term in the analysis. In fact, such modification or stabilization is necessary for the proof of energy decay, which is pointed out in the remark attached to the main theorem. However, the stabilization may cause significant time delay phenomena if a low-order scheme is used or a large time step is taken. We study the effect in detail for higher-order schemes in Section 4. On the other hand, the stabilization is necessary to guarantee the maximum bound property (MBP) for Allen-Cahn equations (see [8]). Besides, [32] provides numerical evidence to illustrate that the stabilization can significantly improve the numerical performance.

2.2 ETDRK methods

The key idea of ETDRK is to consider Duhamel's principle for the equation (2.7), i.e.,

$$u(x,t) = \mathrm{e}^{GL(t-t_0)}u(x,t_0) - \mathrm{e}^{GL(t-t_0)}\int_{t_0}^{t} \mathrm{e}^{-GL(s-t_0)}Gg(u(x,s))ds, \tag{2.8}$$

and approximate the implicit integral with a suitable quadrature formula. For example, assuming that we have u_n, the approximate solution at time step n, we see that the simplest way to determine u_{n+1} is to substitute the function $g(u)$ by a constant $g(u_n)$ which leads to the first-order ETD (ETD1) scheme

$$u_{n+1} = \mathrm{e}^{\tau GL}u_n + (I - \mathrm{e}^{\tau GL})L^{-1}g(u_n), \tag{2.9}$$

where τ is the time step. For this scheme, the energy dissipation law and MBP for the Allen-Cahn equation have been proved (see, e.g., [9]). The classical second-order ETDRK (ETDRK2) for the gradient flow (1.1) reads

$$v = \mathrm{e}^{\tau GL}u_n + (I - \mathrm{e}^{\tau GL})L^{-1}g(u_n), \tag{2.10}$$

$$u_{n+1} = v - \frac{1}{\tau}(\mathrm{e}^{\tau GL} - I - \tau GL)(GL)^{-2}(Gg(v) - Gg(u_n)). \tag{2.11}$$

It is shown in [14] that the above scheme is energy decreasing with a suitably large stabilization constant β for the Allen-Cahn and Cahn-Hilliard equations.

In general, the ETDRK schemes take the following form [7]:

$$\begin{aligned} &v_1 = u_n, \\ &v_i = \chi_i(\tau GL)u_n - \tau\sum_{j=1}^{i-1} a_{ij}(\tau GL)Gg(v_j), \quad i = 2,\dots,s, \\ &u_{n+1} = \chi(\tau GL)u_n - \sum_{j=1}^{s} b_j(\tau GL)Gg(v_j), \end{aligned} \tag{2.12}$$

where $\chi(z) = \mathrm{e}^z$, $\chi_i(z) = \chi(c_i z)$, and the coefficients a_{ij} and b_j are constructed to equal to or approximate exponential functions. For simplicity, we define a class of functions which will be frequently used

$$\phi_0(z) = \mathrm{e}^z, \quad \phi_{k+1}(z) = \frac{\phi_k(z) - \phi_k(0)}{z} \quad \text{with } \phi_k(0) = 1/k!. \tag{2.13}$$

The ETDRK schemes (2.12) could also be written in the Butcher tableau, although now its coefficients are functions

$$\begin{array}{c|ccc|c} c_1 & & & & \chi_1(\tau GL) \\ c_2 & a_{21} & & & \chi_2(\tau GL) \\ \cdots & \cdots & \cdots & & \cdots \\ c_s & a_{s1} & \cdots & a_{s,s-1} & \chi_s(\tau GL) \\ \hline & b_1 & b_2 & \cdots\quad b_s & \chi(\tau GL) \end{array}. \tag{2.14}$$

In order to preserve the equilibria, the coefficients of the method have to satisfy

$$\sum_{j=1}^{s} b_j(z) = \frac{\chi(z)-1}{z}, \quad \sum_{j=1}^{s} a_{ij}(z) = \frac{\chi_i(z)-1}{z}. \tag{2.15}$$

Taking the ETDRK2 as an example, we see that $a_{21}(z) = \phi_1(z) = (\mathrm{e}^z - 1)/z$, $b_2(z) = \phi_2(z) = (\mathrm{e}^z - z - 1)/z^2$, and $b_1 = \phi_1 - \phi_2$, where $z = \tau GL$ and its Butcher tableau reads

$$\begin{array}{c|cc|c} 0 & & & 1 \\ 1 & \phi_1(\tau GL) & & \chi(\tau GL) \\ \hline & \phi_1(\tau GL) - \phi_2(\tau GL) & \phi_2(\tau GL) & \chi(\tau GL) \end{array}. \tag{2.16}$$

With the help of (2.15) and setting $u_{n+1} = v_{s+1}$, we can rewrite the solution (2.12) as

$$\begin{aligned} v_i &= u_n + \tau \sum_{j=1}^{i-1} a_{ij}(\tau GL)(GLu_n - Gg(v_j)), \quad i = 2, \ldots, s, \\ v_{s+1} &= u_n + \tau \sum_{j=1}^{s} b_j(\tau GL)(GLu_n - Gg(v_j)). \end{aligned} \tag{2.17}$$

2.3 A general framework for energy stable ETDRK schemes

We present below a general framework for constructing energy-stable ETDRK schemes. We start with a useful lemma whose proof is straightforward.

Lemma 2.1. *Consider a positive-definite operator $L = \beta I + \mathcal{L}$, and let f be an analytic function whose domain includes the spectrum of L, i.e., the values $\{f(\lambda_i)\}_{i\in\mathcal{N}}$ exist, where $\{\lambda_i\}_{i\in\mathcal{N}}$ are the eigenvalues of L. Then, the eigenvalues of $f(L)$ are $\{f(\lambda_i)\}_{i\in\mathcal{N}}$. Furthermore, if f is a positive function, then $f(L)$ is also a positive-definite operator.*

Hereafter, we say a matrix A is positive-definite if the eigenvalues of its symmetrizer $(A + A^{\mathrm{T}})/2$ are all positive.

Theorem 2.2. *Consider the gradient flow*

$$u_t = G(\mathcal{L}u + f(u)), \quad (x,t) \in \Omega \times [0,T], \tag{2.18}$$

where G is a negative operator, $\mathcal{L}$ is a sectorial operator that commutes with G, and f is a Lipschitz continuous function with the Lipschitz constant C_L. The ETDRK schemes (2.12) *with the stabilizer $\beta \geqslant C_L$ unconditionally decreases the energy as long as the following determinant*

$$\mathcal{D}(z) = zE_L + P^{-1}E_L - \frac{z}{2}I \tag{2.19}$$

is positive-definite for all negative $z \in \mathbb{R}$, where I is the identity operator, $E_L = (1_{i\geqslant j})_{s\times s}$ is the lower

triangular matrix with all nonzero entries equal to 1*, and*

$$P = \begin{pmatrix} a_{21} & & & & \\ a_{31} & a_{32} & & & \\ \vdots & \vdots & \ddots & & \\ a_{s1} & a_{s2} & \cdots & a_{s(s-1)} & \\ b_1 & b_2 & \cdots & b_{s-1} & b_s \end{pmatrix}, \tag{2.20}$$

where a_{ij} *and* b_i *are given in* (2.14)*.*

Proof. We first compute the difference in the energy and derive a key inequality.

Since the function f is Lipschitz continuous, given any v and u, we have

$$\begin{aligned}(F(v) - F(u), 1) &\leqslant (v-u, f(u)) + \frac{C_L}{2}(v-u, v-u) \\ &= -(v-u, g(u)) + \beta(v-u, u) + \frac{C_L}{2}(v-u, v-u).\end{aligned} \tag{2.21}$$

On the other hand,

$$\begin{aligned}\frac{1}{2}\bigg(\int_\Omega |\mathcal{L}_{1/2}v|^2 - |\mathcal{L}_{1/2}u|^2 dx\bigg) &= \frac{1}{2}((v, \mathcal{L}v) - (u, \mathcal{L}u)) \\ &= (v-u, \mathcal{L}v) - \frac{1}{2}(v-u, \mathcal{L}(v-u)) \\ &= (v-u, Lv) - \beta(v-u, v) - \frac{1}{2}(v-u, \mathcal{L}(v-u)),\end{aligned} \tag{2.22}$$

where we used the identity

$$[a,a] - [b,b] = 2[a-b, a] - [a-b, a-b]$$

which is valid for all a, b, and any bilinear form $[\cdot,\cdot]$. Therefore, combining these two parts, we derive

$$E(v) - E(u) \leqslant (v-u, Lv - g(u)) - \frac{1}{2}(v-u, L(v-u)) - \frac{\beta - C_L}{2}(v-u, v-u). \tag{2.23}$$

This vital inequality holds with the Lipschitz condition, and if we take $\beta \geqslant C_L$, the second term is naturally non-positive.

Now we focus on the ETDRK scheme (2.17), the first line of which is $v_1 = u_n$, and the rest can be rewritten as the following system:

$$\begin{pmatrix} v_2 - v_1 \\ v_3 - v_1 \\ \vdots \\ v_{s+1} - v_1 \end{pmatrix} = \tau P \begin{pmatrix} G(Lv_1 - g(v_1)) \\ G(Lv_1 - g(v_2)) \\ \vdots \\ G(Lv_1 - g(v_s)) \end{pmatrix}, \tag{2.24}$$

which is equivalent to

$$\begin{pmatrix} Lv_1 - g(v_1) \\ Lv_1 - g(v_2) \\ \vdots \\ Lv_1 - g(v_s) \end{pmatrix} = \frac{1}{\tau}P^{-1} \begin{pmatrix} G^{-1}(v_2 - v_1) \\ G^{-1}(v_3 - v_1) \\ \vdots \\ G^{-1}(v_{s+1} - v_1) \end{pmatrix} = \frac{1}{\tau}P^{-1}E_L \begin{pmatrix} G^{-1}(v_2 - v_1) \\ G^{-1}(v_3 - v_2) \\ \vdots \\ G^{-1}(v_{s+1} - v_s) \end{pmatrix}. \tag{2.25}$$

Therefore,

$$E(u_{n+1}) - E(u_n)$$

$$
\begin{aligned}
&= \sum_{k=1}^{s}(E(v_{k+1}) - E(v_k)) \\
&\leqslant \sum_{k=1}^{s}(v_{k+1}-v_k, Lv_{k+1} - g(v_k)) - \frac{1}{2}\sum_{k=1}^{s}(v_{k+1}-v_k, L(v_{k+1}-v_k)) - \frac{\beta - C_L}{2}\sum_{k=1}^{s}\|v_{k+1}-v_k\|^2 \\
&= \sum_{k=1}^{s}((v_{k+1}-v_k, Lv_{k+1} - Lv_1) + (v_{k+1}-v_k, Lv_1 - g(v_k))) \\
&\quad - \frac{1}{2}\sum_{k=1}^{s}(v_{k+1}-v_k, L(v_{k+1}-v_k)) - \frac{\beta - C_L}{2}\sum_{k=1}^{s}\|v_{k+1}-v_k\|^2 \\
&= \sum_{k=1}^{s}\left(\left(v_{k+1}-v_k, \frac{1}{\tau}G^{-1}(\tau GL)\sum_{j=1}^{k}(v_{j+1}-v_j)\right) + (v_{k+1}-v_k, Lv_1 - g(v_k))\right) \\
&\quad -\frac{1}{2}\sum_{k=1}^{s}\left(v_{k+1}-v_k, \frac{1}{\tau}G^{-1}(\tau GL)(v_{k+1}-v_k)\right) - \frac{\beta - C_L}{2}\sum_{k=1}^{s}\|v_{k+1}-v_k\|^2 \text{ (using (2.25))} \\
&= \frac{1}{\tau}\sum_{k=1}^{s}\sum_{j=1}^{k}((v_{k+1}-v_k, G^{-1}(\tau GL)(v_{j+1}-v_j)) + (v_{k+1}-v_k, G^{-1}(P^{-1}E_L)_{kj}(v_{j+1}-v_j))) \\
&\quad - \frac{1}{2\tau}\sum_{k=1}^{s}(v_{k+1}-v_k, G^{-1}(\tau GL)(v_{k+1}-v_k)) - \frac{\beta - C_L}{2}\sum_{k=1}^{s}\|v_{k+1}-v_k\|^2 \\
&= \frac{1}{\tau}\sum_{k,j=1}^{s}(v_{k+1}-v_k, G^{-1}\mathcal{D}_{kj}(\tau GL)(v_{j+1}-v_j)) - \frac{\beta - C_L}{2}\sum_{k=1}^{s}\|v_{k+1}-v_k\|^2, \qquad (2.26)
\end{aligned}
$$

where $\mathcal{D}(z) = zE_L + P^{-1}E_L - \frac{z}{2}I$ with $z = \tau GL$. Since G is a negative operator and $\beta \geqslant C_L$, the discrete energy unconditionally decreases if $\mathcal{D}(z)$ is positive-definite for all negative $z \in \mathbb{R}$. □

Remark 2.3. For the MBE model, recall that the nonlinear term is Lipschitz continuous as a function of ∇u, and meanwhile, the convex splitting of the energy is also different (see [23, 39] for more details). However, all the analyses in the proof can be carried out in a similar way. To keep the presentation short, we omit the proof.

Remark 2.4. The inequality (2.23) in the proof plays a very important role. It is the only place where we apply the Lipschitz condition. Alternatively, we can also replace the Lipschitz condition with a convex splitting approach since

$$
\begin{aligned}
E(v) - E(u) &\leqslant \left(v-u, \frac{\delta E_l}{\delta v}(v) - \frac{\delta E_n}{\delta u}(u)\right) \\
&= (v-u, \mathcal{L}v + f(u)) \\
&= (v-u, Lv - g(u)). \qquad (2.27)
\end{aligned}
$$

The determinant of this version is slightly different, while the rest of the proof is the same.

Lemma 2.5. *The positive-definiteness of* $\frac{1}{2}(\mathcal{D} + \mathcal{D}^{\mathrm{T}})$ *is equivalent to the positive-definiteness of*

$$\mathcal{D}' = zPE_AP^{\mathrm{T}} + E_LP^{\mathrm{T}} + PE_L^{\mathrm{T}},$$

where E_A *is the matrix of all ones.*

Proof. Notice that

$$E_L + E_L^{\mathrm{T}} = E_A + I$$

and

$$P(\mathcal{D} + \mathcal{D}^{\mathrm{T}})P^{\mathrm{T}} = zP(E_L + E_L^{\mathrm{T}} - I)P^{\mathrm{T}} + E_LP^{\mathrm{T}} + PE_L^{\mathrm{T}} = \mathcal{D}'.$$

This completes the proof. □

Remark 2.6. $\mathcal{D}'$ is already symmetric and helps us in the understanding and subsequent proof regarding positive-definiteness.

3 Examples of energy decreasing ETDRK schemes

In this section, we consider some examples of ETDRK methods up to order four.

We first recall

$$\phi_0(z) = \mathrm{e}^z, \quad \phi_{k+1} = \frac{\phi_k(z) - \phi_k(0)}{z}, \quad \phi_k(0) = \frac{1}{k!}. \tag{3.1}$$

We also define $\phi_{i,j}(z) = \phi_i(c_j z)$ for simplicity.

3.1 The first-order ETD scheme

We start with a very simple ETD1 scheme

$$u_{n+1} = \mathrm{e}^{\tau GL} u_n + (I - \mathrm{e}^{\tau GL}) L^{-1} g(u_n), \tag{3.2}$$

whose Butcher tableau reads

$$\begin{array}{c|c} 0 & 0 \\ \hline & \phi_1(\tau GL) \end{array}. \tag{3.3}$$

Corollary 3.1. *The first-order ETD scheme unconditionally decreases the discrete energy.*

Proof. The only element in P is $b_1 = \phi_1$, whence the determinant

$$\mathcal{D}(z) = z + 1/\phi_1(z) - z/2 = z\mathrm{e}^z/(\mathrm{e}^z - 1) - z/2.$$

Therefore, $\mathcal{D} \geqslant 0$ always holds for $z \leqslant 0$. Theorem 2.2 guarantees that the discrete energy of the ETD1 solution unconditionally decreases. □

3.2 The Second-order ETDRK scheme

In [14], it has been proved that the following ETDRK2 scheme is unconditionally energy stable, while here we could make use of the framework to obtain the same result. In fact, the estimate here is finer than the result in [14].

We consider the following ETDRK2 scheme:

$$v = \mathrm{e}^{\tau GL} u_n + (I - \mathrm{e}^{\tau GL}) L^{-1} g(u_n), \tag{3.4}$$

$$u_{n+1} = v - \frac{1}{\tau}(\mathrm{e}^{\tau GL} - I - \tau GL)(GL)^{-2}(Gg(v) - Gg(u_n)). \tag{3.5}$$

The Butcher tableau reads

$$\begin{array}{c|cc} 0 & 0 & \\ 1 & \phi_1 & \\ \hline & \phi_1 - \phi_2 & \phi_2 \end{array}. \tag{3.6}$$

Corollary 3.2. *The second-order ETDRK scheme unconditionally decreases the discrete energy.*

Proof. According to the Butcher tableau, we have

$$P = \begin{pmatrix} \phi_1 & 0 \\ \phi_1 - \phi_2 & \phi_2 \end{pmatrix}, \quad P^{-1} = \begin{pmatrix} 1/\phi_1 & 0 \\ (\phi_2 - \phi_1)/(\phi_1\phi_2) & 1/\phi_2 \end{pmatrix},$$

whence the determinant reads

$$\mathcal{D}(z) = \begin{pmatrix} z + 1/\phi_1 & 0 \\ z + 1/\phi_1 & z + 1/\phi_2 \end{pmatrix} - \frac{z}{2} I_2 = (z + 1/\phi_1) E_L + \begin{pmatrix} 0 & 0 \\ 0 & 1/\phi_2 - 1/\phi_1 \end{pmatrix} - \frac{z}{2} I_2. \tag{3.7}$$

The first term is positive-definite since $(z + 1/\phi_1)$ is positive and E_L is positive-definite, the second term is also non-negative-definite because $\phi_1 > \phi_2 > 0$, and the third term is obviously positive-definite. Therefore, $\mathcal{D}$ is positive-definite, and the ETDRK2 scheme is unconditionally energy stable. □

3.3 Third-order ETDRK schemes

In general, third-order ETDRK schemes need to satisfy the following order conditions:

Order	Conditions
1	$\psi_1 = 0$
2	$\psi_2 = 0$
2	$\psi_{1,i} = 0$
3	$\psi_3 = 0$
3	$\sum_{i=1}^{s} b_i J\psi_{2,i} = 0$

where

$$\psi_i(z) = \phi_i(z) - \sum_{k=1}^{s} b_k c_k^{j-1}/(j-1)!, \quad \psi_{i,j} = \phi_i c_j^i - \sum_{k=1}^{j-1} a_{jk} c_k^{i-1}/(i-1)!, \tag{3.8}$$

and J denotes arbitrary bounded operators. In particular, the classical ETDRK3 scheme below from Cox and Matthews [7] does not satisfy the conditions of our theorem (see Figure 1), so it is not unconditionally energy decreasing. It holds that

$$\begin{array}{c|ccc} 0 & & & \\ \frac{1}{2} & \frac{1}{2}\phi_{1,2} & & \\ 1 & -\phi_{1,3} & 2\phi_{1,3} & \\ \hline & 4\phi_3 - 3\phi_2 + \phi_1 & -8\phi_3 + 4\phi_2 & 4\phi_3 - \phi_2 \end{array}. \tag{3.9}$$

On the other hand, all the possible types of three-stage third-order ETDRK schemes are listed in [17,18]. In fact, many of them with suitable coefficients could satisfy the requirement of our theorem, and two of them are described with the Butcher tableau below:

$$\begin{array}{c|ccc} 0 & & & \\ 1 & \phi_1 & & \\ \frac{2}{3} & \frac{2}{3}\phi_{1,3} - \frac{4}{9}\phi_{2,3} & \frac{4}{9}\phi_{2,3} & \\ \hline & \frac{3}{4}\phi_1 - \phi_2 & \phi_2 - \frac{1}{2}\phi_1 & \frac{3}{4}\phi_1 \end{array} \tag{3.10}$$

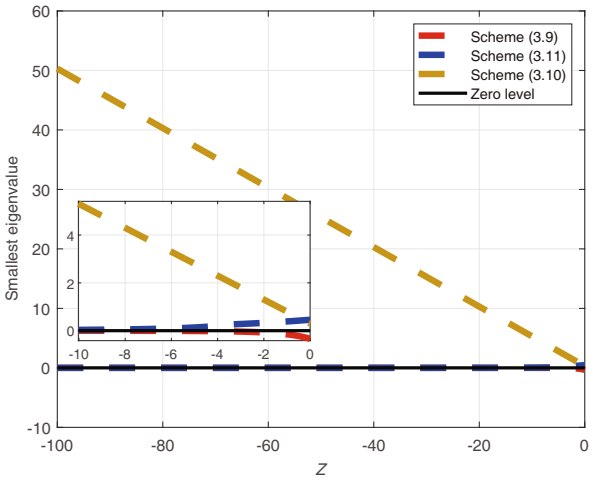

Figure 1 (Color online) Eigenvalues of $\frac{1}{2}(\mathcal{D} + \mathcal{D}^{\mathrm{T}})$ for the three ETDRK3 schemes

and

$$\begin{array}{c|ccc} 0 & & & \\ \frac{4}{9} & \frac{4}{9}\phi_{1,2} & & \\ \frac{2}{3} & \frac{2}{3}\phi_{1,3}-\phi_{2,3} & \phi_{2,3} & \\ \hline & \phi_1-\frac{3}{2}\phi_2 & 0 & \frac{3}{2}\phi_2 \end{array}. \tag{3.11}$$

To begin with, we first present numerical evidences. We plot in Figure 1 the smallest eigenvalues of $\frac{1}{2}(\mathcal{D}+\mathcal{D}^{\mathrm{T}})$ for the three schemes above, and we observe that the smallest eigenvalues of (3.10) and (3.11) are positive, indicating that the conditions of our theorem are satisfied. In contrast, the smallest eigenvalues for the scheme (3.9) become negative when z approaches zero, indicating that the conditions of our theorem are violated. To rigorously show that the above two ETDRK schemes decrease the energy, we only need to prove the positive-definiteness of $\mathcal{D}'$ for the above schemes, which could be verified by checking all the leading principal minors. Here, we want to point out that it does not necessarily mean that schemes which violate the conditions are not energy dissipative since in our theorem they are solely sufficient conditions.

Proposition 3.3. *For the schemes* (3.10) *and* (3.11)*, the determinants of all the leading principal minors of* $\mathcal{D}'$ *are positive, and thus* $\mathcal{D}'$ *is positive definite. Thus, the schemes* (3.10) *and* (3.11) *unconditionally decrease the energy for the general gradient flow* (2.7)*.*

Proof. According to (3.10), we derive the expressions for the determinants of leading principal minors as follows

$$\begin{aligned}
\mathrm{Det}(\mathcal{D}'_{1\times1}) &= \mathcal{D}'_{11} = \frac{\mathrm{e}^z-1}{z} > 0,\\
\mathrm{Det}(\mathcal{D}'_{2\times2}) &= \frac{1}{9z^4}(-9\mathrm{e}^{4z/3}+18\mathrm{e}^{2z/3}+6z-6z\mathrm{e}^{2z/3}-18z\mathrm{e}^{5z/3}+18z\mathrm{e}^{7z/3}-9z^2\mathrm{e}^{2z}-9z^2\mathrm{e}^{4z/3}\\
&\quad +6z^2\mathrm{e}^{5z/3}+8z^2-9),\\
\mathrm{Det}(\mathcal{D}') &= \frac{1}{36z^6}(252z+162\mathrm{e}^{2z}-162\mathrm{e}^{2z/3}+324\mathrm{e}^{5z/3}-162\mathrm{e}^{8z/3}-324\mathrm{e}^{z}+99z\mathrm{e}^{2z}+54z\mathrm{e}^{3z}\\
&\quad -81z\mathrm{e}^{4z}-180z\mathrm{e}^{2z/3}-45z\mathrm{e}^{4z/3}+378z\mathrm{e}^{5z/3}+54z\mathrm{e}^{7z/3}-468z\mathrm{e}^{8z/3}-9z\mathrm{e}^{10z/3}\\
&\quad +270z\mathrm{e}^{11z/3}-72z^2\mathrm{e}^{z}+78z^2\mathrm{e}^{2z}-18z^2\mathrm{e}^{3z}+83z^3\mathrm{e}^{2z}+6z^2\mathrm{e}^{2z/3}-54z^2\mathrm{e}^{4z/3}\\
&\quad +288z^2\mathrm{e}^{5z/3}+27z^3\mathrm{e}^{4z/3}+18z^3\mathrm{e}^{5z/3}-54z^2\mathrm{e}^{7z/3}-240z^2\mathrm{e}^{8z/3}-324z\mathrm{e}^{z}+66z^2\\
&\quad -20z^3+162).
\end{aligned}$$

It can be verified by Figure 2 that for z with small absolute values,

$$\begin{aligned}
&z^4\mathrm{Det}(\mathcal{D}'_{2\times2}) \geqslant 0.2, \quad z\in[-3,-1], \quad \mathrm{Det}(\mathcal{D}'_{2\times2}) \geqslant 0.2, \quad \forall\, z\in[-1,0),\\
&z^6\mathrm{Det}(\mathcal{D}') \geqslant 0.1, \quad z\in[-6,-1], \quad \mathrm{Det}(\mathcal{D}') \geqslant 0.1, \quad \forall\, z\in[-1,0),
\end{aligned}$$

where both $z^4\mathrm{Det}(\mathcal{D}')_{2\times2}$ and $z^6\mathrm{Det}(\mathcal{D}')$ are smooth decreasing functions and both $\mathrm{Det}(\mathcal{D}')_{2\times2}$ and $\mathrm{Det}(\mathcal{D}')$ are smooth increasing functions.

For z with large scales, we use the non-exponential term to control the exponentially small term. Therefore, we denote the non-exponential term in $z^4\mathrm{Det}(\mathcal{D}'_{2\times2})$ as $P_2 = (6z+8z^2-9)/9$ and the exponential term as

$$R_2 = (-9\mathrm{e}^{4z/3}+18\mathrm{e}^{2z/3}-6z\mathrm{e}^{2z/3}-18z\mathrm{e}^{5z/3}+18z\mathrm{e}^{7z/3}-9z^2\mathrm{e}^{2z}-9z^2\mathrm{e}^{4z/3}+6z^2\mathrm{e}^{5z/3})/9.$$

When $z<-3$,

$$\begin{aligned}
&P_2(z) > P_2(-3) = 6,\\
&|R_2| < (9\mathrm{e}^{-4}+18\mathrm{e}^{-2}+6\times3\mathrm{e}^{-2}+18\times3\mathrm{e}^{-5}+18\times3\mathrm{e}^{-7}+9\times3^2\mathrm{e}^{-2}+9\times3^2\mathrm{e}^{-4}+6\times3^2\mathrm{e}^{-5})/9\\
&\qquad < 2.03,
\end{aligned}$$

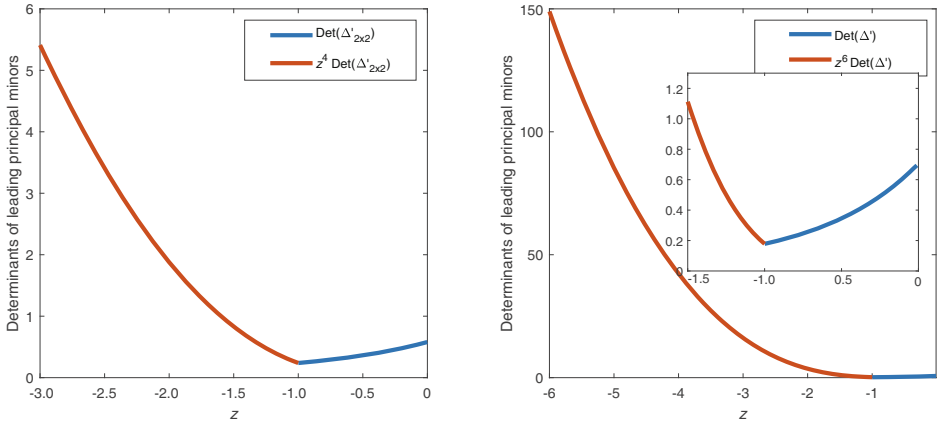

Figure 2 (Color online) Positive-definiteness test: Determinants of leading principal minors

where we use $\beta \leqslant |\beta|$ for every single term in R_2. Thus, $z^4\mathrm{Det}(\mathcal{D}'_{2\times 2}) \geqslant P_2 - |R_2| > 6 - 2.03 > 0$ for all $z < -3$.

Similarly, we define the non-exponential term P_3 and the exponential term R_3 for $z^6\mathrm{Det}(\mathcal{D})$, and for $z < -6$, we have $P_3(z) > P_3(-6) = 148.5$ and $|R_3(z)| < 86$, and thus $z^6\mathrm{Det}(\mathcal{D}') > P_3(z) - |R_3(z)| > 0$. Combining all the above results, we have $\mathrm{Det}(\mathcal{D}'_{2\times 2}) > 0$, and $\mathrm{Det}(\mathcal{D}') > 0$ for all negative z.

Therefore, all the determinants of leading principal minors are positive, i.e., $\mathcal{D}'$ is positive-definite.

For the scheme (3.11), the proof is the same and we just present the determinants of leading principal minors here:

$$
\begin{aligned}
\mathrm{Det}(\mathcal{D}'_{1\times 1}) &= \mathcal{D}'_{11} = \frac{\mathrm{e}^{8z/9}-1}{z} > 0,\\
\mathrm{Det}(\mathcal{D}'_{2\times 2}) &= -\frac{1}{16z^4}(36z - 162\mathrm{e}^{2z/3} + 81\mathrm{e}^{4z/3} - 36z\mathrm{e}^{2z/3}\\
&\quad + 72z\mathrm{e}^{10z/9} - 72z\mathrm{e}^{16z/9} + 16z^2\mathrm{e}^{4z/3} + 16z^2\mathrm{e}^{8z/9} + 16z^2\mathrm{e}^{10z/9} - 12z^2 + 81),\\
\mathrm{Det}(\mathcal{D}') &= -\frac{1}{32z^5}(22\mathrm{e}^{2z} - 71z + 288\mathrm{e}^{2z/3} - 130\mathrm{e}^{4z/3} - 216\mathrm{e}^{5z/3} + 80\mathrm{e}^{7z/3} - 72\mathrm{e}^{8z/3} + 50\mathrm{e}^{10z/3}\\
&\quad + 136\mathrm{e}^{z} + 5z\mathrm{e}^{2z} + 63z\mathrm{e}^{2z/3} + 16z\mathrm{e}^{4z/3} - 86z\mathrm{e}^{5z/3} + 4z\mathrm{e}^{7z/3} + 23z\mathrm{e}^{8z/3} - 20z\mathrm{e}^{10z/3}\\
&\quad - 128z\mathrm{e}^{10z/9} - 28z\mathrm{e}^{13z/9} + 144z\mathrm{e}^{16z/9} - 4z\mathrm{e}^{19z/9} + 172z\mathrm{e}^{22z/9} - 156z\mathrm{e}^{28z/9} - 4z^2\mathrm{e}^{z}\\
&\quad - 50z^2\mathrm{e}^{2z} - 30z^2\mathrm{e}^{4z/3} + 8z^2\mathrm{e}^{5z/3} - 4z^2\mathrm{e}^{7z/3} + 56z^2\mathrm{e}^{8z/3} + 2z^2\mathrm{e}^{10z/3} - 30z^2\mathrm{e}^{8z/9}\\
&\quad - 28z^2\mathrm{e}^{10z/9} - 8z^2\mathrm{e}^{13z/9} + 12z^2\mathrm{e}^{17z/9} + 8z^2\mathrm{e}^{19z/9} + 40z^2\mathrm{e}^{22z/9} + 18z^2\mathrm{e}^{26z/9}\\
&\quad - 12z^2\mathrm{e}^{28z/9} + 66z\mathrm{e}^{z} + 22z^2 - 158).
\end{aligned}
$$

This completes the proof. □

Since the scheme (3.10) has the largest positive smallest eigenvalue according to the following Figure 1, we use it to represent energy stable ETDRK3 for numerical tests in Section 4.

3.4 Fourth-order ETDRK schemes

In general, fourth-order ETDRK schemes need to satisfy four more order conditions:

Order	Conditions
4	$\psi_4 = 0$
4	$\sum_{i=1}^{s} b_i J\psi_{3,i} = 0$
4	$\sum_{i=1}^{s} b_i J \sum_{j=2}^{i-1} a_{ij} J\psi_{2,j} = 0$
4	$\sum_{i=1}^{s} b_i c_i K\psi_{2,i} = 0$

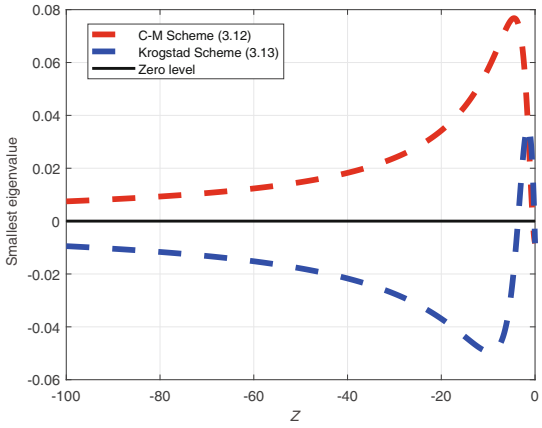

Figure 3 (Color online) Eigenvalues of ETDRK4 schemes from Cox and Mathhews [7] and Krogstad [22]

where

$$\psi_i(z) = \phi_i(z) - \sum_{k=1}^{s} b_k c_k^{j-1}/(j-1)!, \quad \psi_{i,j} = \phi_i c_j^i - \sum_{k=1}^{j-1} a_{jk} c_k^{i-1}/(i-1)!,$$

and J and K denote arbitrary bounded operators (see, for more details, [18]). These fourth-order conditions are more complicated than previous third-order conditions so that it is more difficult to construct fourth-order ETDRK schemes. One of the most used ETDRK4 schemes is from Cox and Matthews [7]:

$$\begin{array}{c|cccc} 0 & & & & \\ \frac{1}{2} & \frac{1}{2}\phi_{1,2} & & & \\ \frac{1}{2} & 0 & \frac{1}{2}\phi_{1,3} & & \\ 1 & \frac{1}{2}\phi_{1,3}(\phi_{0,3}-1) & 0 & \phi_{1,3} & \\ \hline & \phi_1 - 3\phi_2 + 4\phi_3 & 2\phi_2 - 4\phi_3 & 2\phi_2 - 4\phi_3 & 4\phi_3 - \phi_2 \end{array}. \tag{3.12}$$

The other is given by Krogstad [22]:

$$\begin{array}{c|cccc} 0 & & & & \\ \frac{1}{2} & \frac{1}{2}\phi_{1,2} & & & \\ \frac{1}{2} & \frac{1}{2}\phi_{1,3} - \phi_{2,3} & \phi_{2,3} & & \\ 1 & \phi_{1,4} - 2\phi_{2,4} & 0 & 2\phi_{2,4} & \\ \hline & \phi_1 - 3\phi_2 + 4\phi_3 & 2\phi_2 - 4\phi_3 & 2\phi_2 - 4\phi_3 & 4\phi_3 - \phi_2 \end{array}. \tag{3.13}$$

We plot in Figure 3 the smallest eigenvalues of $\frac{1}{2}(\mathcal{D} + \mathcal{D}^{\mathrm{T}})$ for the two schemes above, the results clearly indicate that the above two schemes do not satisfy our conditions for energy stability. Moreover, we checked all the existing fourth-order ETDRK schemes and also searched from a wide family of four-stage and five-stage fourth-order ETDRK methods, but none of them satisfies the requirement of our theorem. Therefore, the existence of energy-stable ETDRK4 schemes is still an open problem.

4 Numerical experiments

In this section, we carry out some numerical experiments to illustrate the convergence and energy decay property of our new ETDRK schemes for different phase-field models. We first verify the temporal convergence rates using smooth initial data for the Allen-Cahn and Cahn-Hilliard equations. Next, we study the behavior with large time steps for the Allen-Cahn, Cahn-Hilliard, and phase field crystal

equations. Then, we present energy curves for different time steps and stabilization constants to observe their influence. Finally, we present an adaptive time-stepping strategy that takes advantage of the unconditional energy stability.

In all the simulations, we consider models with periodic conditions and use a Fourier-spectral method in space with a sufficiently fine mesh so that the spatial discretization errors can be ignored compared with temporal discretization errors. The ETDRK3 scheme (3.10) is used if not specified otherwise. Besides, we also consider a truncated double-well potential $\tilde{F}(u)$ so that it naturally satisfies the Lipschitz condition. More precisely, for a sufficiently large M ($M = 2$ is enough for cases used in this paper), we replace $F(u) = \frac{1}{4}(u^2-1)^2$ by

$$\tilde{F}(u) = \begin{cases} \dfrac{3M^2-1}{2}u^2 - 2\mathrm{sgn}(u)M^3u + \dfrac{1}{4}(3M^4+1), & |u| > M, \\ \dfrac{1}{4}(u^2-1)^2, & |u| \leqslant M, \end{cases}$$

and $f(u) = u^3 - u$ by

$$\tilde{f}(u) = \tilde{F}'(u) = \begin{cases} (3M^2-1)u - 2\mathrm{sgn}(u)M^3, & |u| > M, \\ u^3 - u, & |u| \leqslant M. \end{cases}$$

In fact, the maximum norm of numerical solutions never exceeds the bound M so this replacement does not affect the properties of numerical solutions.

4.1 Convergence tests

We solve the Allen-Cahn and Cahn-Hilliard equations in $\Omega = (0, 2\pi) \times (0, 2\pi)$ with the smooth initial data $u_0 = 0.5 \sin x \sin y$. To compute the errors and the convergence rate, we take the number of grid points $N = 128$ and the interfacial parameter $\epsilon = 0.5$ and set the final time $T = 0.32$. With these settings, we compute the numerical solutions with various time steps $\tau = 0.01/2^k$ with $k = 0, 1, \ldots, 4$ and calculate the relative errors to get the convergence rate. The results for the Allen-Cahn and Cahn-Hilliard equations are listed in Tables 1 and 2, respectively. In both cases, desired convergence rates are observed.

Table 1 ETDRK3 errors and convergence rates for the Allen-Cahn equation

$\tau = 0.01$	L^∞ err	Rate	L^2 err	Rate
τ	2.6852E−08	–	2.0736E−09	–
$\tau/2$	3.4044E−09	2.9795	2.6291E−10	2.9795
$\tau/4$	4.2863E−10	2.9896	3.3101E−11	2.9896
$\tau/8$	5.3815E−11	2.9936	4.1557E−12	2.9937
$\tau/16$	6.7815E−12	2.9883	5.2341E−13	2.9891

Table 2 ETDRK3 errors and convergence rates for the Cahn-Hilliard equation

$\tau = 0.01$	L^∞ err	Rate	L^2 err	Rate
τ	4.2646E−07	–	3.7881E−08	–
$\tau/2$	5.3484E−08	2.9952	4.8765E−09	2.9576
$\tau/4$	6.6767E−09	3.0019	6.1872E−10	2.9785
$\tau/8$	8.3316E−10	3.0025	7.7913E−11	2.9894
$\tau/16$	1.0392E−10	3.0032	9.7637E−12	2.9964

4.2 Large time step tests

In this subsection, we study the accuracy of solutions with large time steps. We set $N = 128$, $T = 8$, $\epsilon = 0.1$ for the Allen-Cahn equation, and $\epsilon = 0.5$ for the Cahn-Hilliard equation. We plot in Figure 4 the relation between the error and the time steps $\tau = 2^{1-k}$ for $k = 0, 1, \ldots, 7$ and observe that the solutions with large time steps still maintain good accuracy.

Next, we simulate the phase field crystal model with $N = 256$, $\epsilon = 0.025$, and $\beta = 3$ in $\Omega = (0, 32) \times (0, 32)$. Using both ETDRK2 and ETDRK3 with the initial condition

$$u_0 = \sin\left(\frac{\pi x}{16}\right) \sin\left(\frac{\pi x}{16}\right),$$

we compute the solution at $T = 1$ with $\tau = 2^{-k}$ for $k = 0, 1, \ldots, 11$. The results are plotted in Figure 5. We observe that both ETDRK schemes work well with large time steps. More precisely, with $\tau = 0.1$, the errors of ETDRK3 and ETDRK2 are about $O(10^{-4})$ and $O(10^{-3})$, respectively.

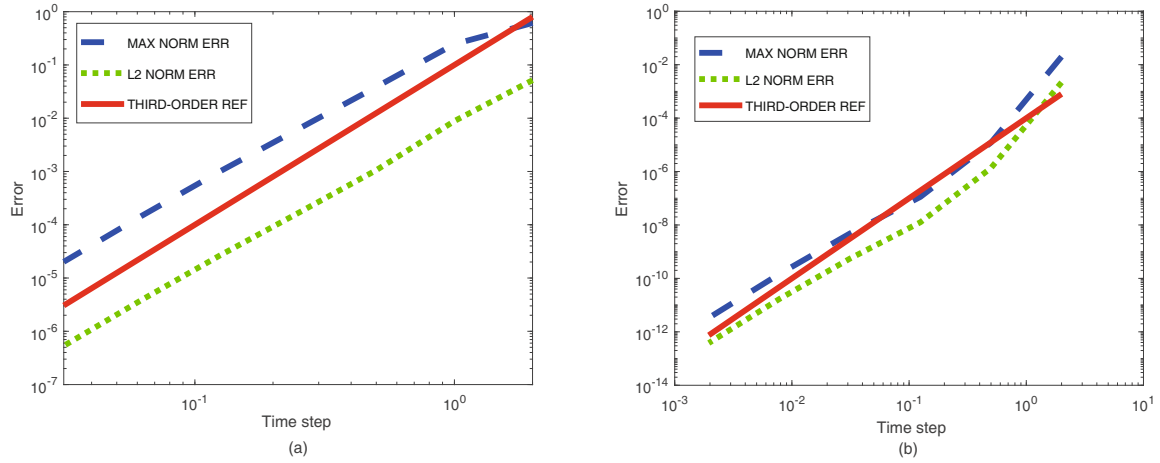

Figure 4 (Color online) Error-τ figure for the AC (a) and CH (b)

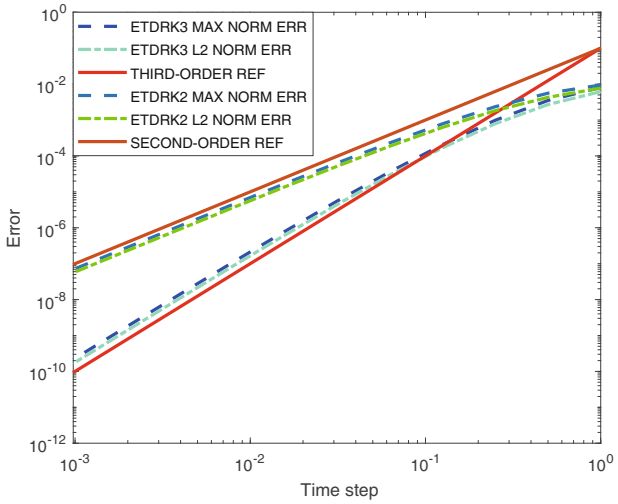

Figure 5 (Color online) Error-τ figure for the phase-field crystal model

4.3 Energy curves with different time steps and stabilization constants

Now we study how energy curves behave with different time steps and stabilization constants. It is well known that stabilization may affect the dynamics and cause serious time delay phenomena when lower-order schemes are used or large time steps are taken. We first test the Cahn-Hilliard equation with $N = 128$, $\epsilon = 0.1$, and $\beta = 2$. The results are presented in Figure 6. We observe that when time steps are large, the time delay phenomena are obvious, but with smaller time steps $\tau \leqslant 0.01$, the influence becomes negligible.

Next, we examine the effect of different stabilization constants. Although theoretically they have to be larger than the Lipschitz constant, we can still run the simulation with smaller stabilization constants. While smaller stabilization constants cause less time delay, solutions may lose their accuracy and even blow-up. Figure 7 shows that when $\tau = 0.1$, the solutions are all inaccurate and exhibit obvious time delays with the solution for $\beta = 0.1$ even showing nonphysical oscillations. This evidence indicates that the stabilization does help the numerical solutions to maintain stability. When $\tau = 0.01$, all three curves with $\beta = 0.1, 1, 2$ are very close, which indicates that the stabilization has very little effect when the time step is small.

4.4 Long time behavior of the phase field crystal model

We simulate in this subsection the long time evolution of the phase field crystal (PFC) model with

$$N = 256, \quad \epsilon = 0.025, \quad \Omega = (0, 128) \times (0, 128),$$

and the initial condition

$$u_0 = 0.05 + 0.01 * \mathrm{rand}(x), \quad x \in \Omega, \tag{4.1}$$

where $\mathrm{rand}(x)$ is a uniformly distributed random function satisfying $-1 \leqslant \mathrm{rand}(x) \leqslant 1$. The long time behavior of the solution obtained by ETDRK3 with $\beta = 3$ and $\tau = 0.1$ is presented in Figure 8.

The energy curves with different time steps and stabilization constants are shown in Figure 9. There are 5 curves in total and 4 of them overlap. With $\beta = 3$, the solution is good when $\tau = 0.1$, but when $\tau = 1$, the time delay caused by the stabilization is much more severe, which indicates that we should not use any stabilization when computing with large time steps. However, it is remarkable that ETDRK3 without stabilization performs very well even with the time step as large as $\tau = 10$.

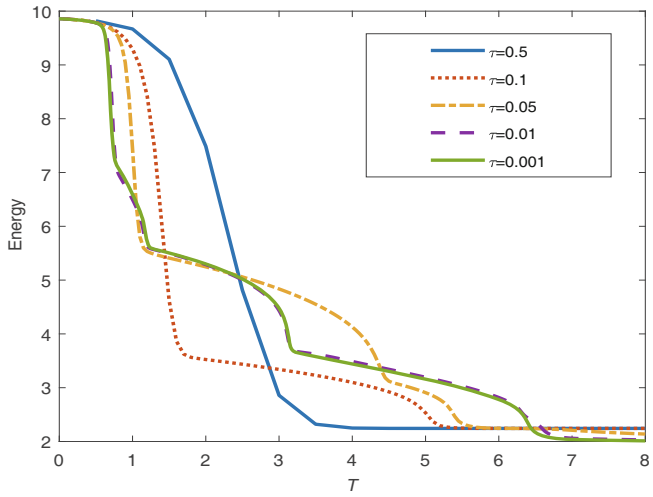

Figure 6 (Color online) Energy curves with different time steps for the Cahn-Hilliard equation

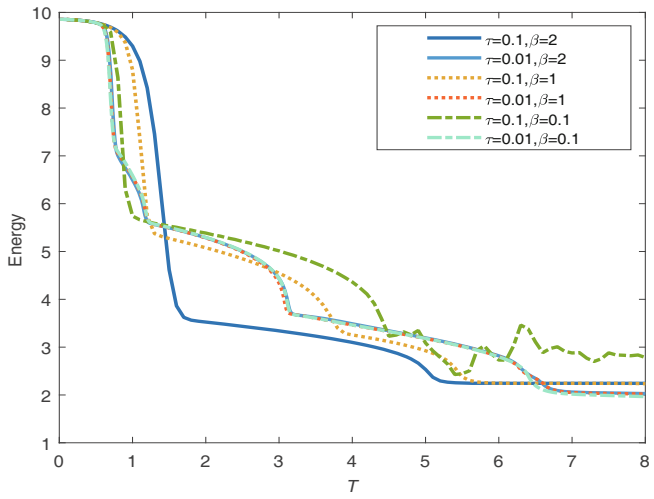

Figure 7 (Color online) Energy curves with different time steps and stabilization constants for the Cahn-Hilliard model

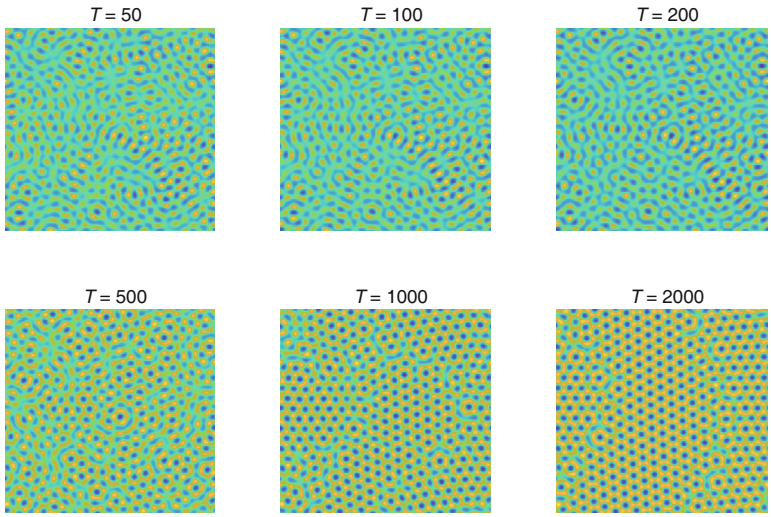

Figure 8 (Color online) ETDRK3 solutions for the PFC model with $\beta = 3, \tau = 0.1$ at $T = 50, 100, 200, 500, 1000, 2000$

4.5 Adaptive time stepping

Solutions of gradient flows may vary drastically during some short time intervals, but change only slightly at other times. A main advantage of unconditional energy stable schemes is that they can be easily used with an adaptive time stepping algorithm, in which the time step is only dictated by accuracy rather than by stability. There are often essential difficulties in applying adaptive time-stepping strategies to other schemes since most of them do not have robust unconditional stability with variable step sizes. This is also where the significance of the high-order unconditional energy stable schemes lies.

For gradient flows, there are several effective adaptive time stepping strategies (see [4,16,29,42]). Here, we make use of the strategy in [30] summarized in the following Algorithm 1. In Steps 4 and 6, the time step size is given by the formula

$$A_{dp}(e,\tau) = \rho\left(\frac{\text{tol}}{e}\right)^{r}\tau, \tag{4.2}$$

along with the restriction of the minimum and maximum time steps. In the above formula, ρ is a default safety coefficient, tol is a reference tolerance, e is the relative error computed at each time level in

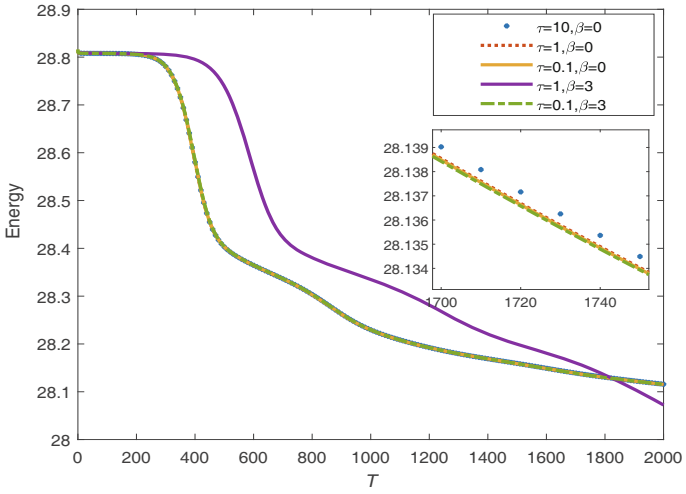

Figure 9 (Color online) Energy curves with different time steps and stabilizers

Step 3, and r is the adaptive rate. In our numerical examples, we set $\rho = 0.9$ and $\text{tol} = 5 * 10^{-3}$, and the minimum time step is 10^{-4}, while the maximum time step is $\tau = 10^{-2}$ for Figures 10 and 11. The initial time step is taken as the minimum time step.

Algorithm 1 Adaptive time stepping procedure

Given: U^n, τ_n
Step 1. Compute U_1^{n+1} by the first-order ETD scheme with τ_n.
Step 2. Compute U_2^{n+1} by the third-order ETDRK scheme with τ_n.
Step 3. Calculate $e_{n+1} = \frac{\|U_1^{n+1} - U_2^{n+1}\|}{\|U_2^{n+1}\|}$.
Step 4. If $e_{n+1} > \text{tol}$, recalculate the time step $\tau_n \leftarrow \max\{\tau_{\min}, \min\{A_{dp}(e_{n+1}, \tau_n), \tau_{\max}\}\}$,
Step 5. goto Step 1.
Step 6. else, update the time step $\tau_{n+1} \leftarrow \max\{\tau_{\min}, \min\{A_{dp}(e_{n+1}, \tau_n), \tau_{\max}\}\}$.
Step 7. endif

We take the two-dimensional Cahn-Hilliard equation as an example to examine the performance of the adaptive time-stepping algorithm. We take $\epsilon = 0.1$, $N = 512$, $\beta = 2$, and $r = 1/3$. As a comparison, we compute two ETDRK3 solutions with a small uniform time step $\tau = 10^{-4}$ and a large uniform time step $\tau = 10^{-2}$ as references.

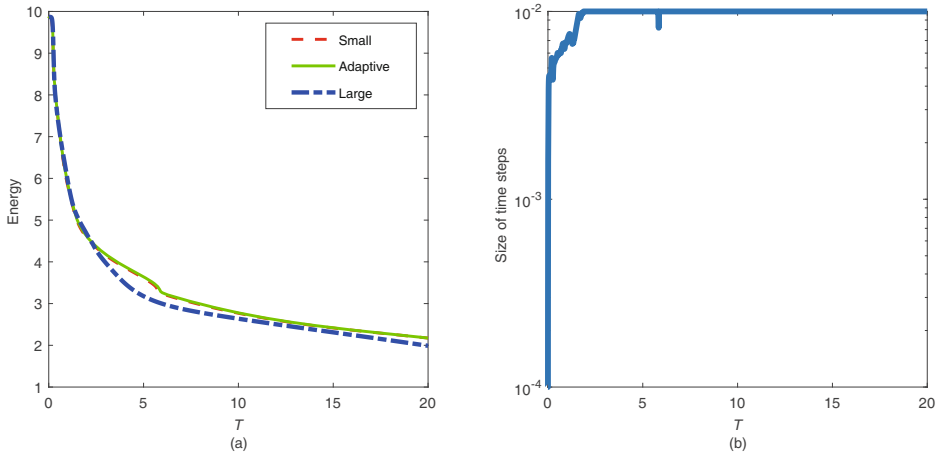

Figure 10 (Color online) Energy curves among small time steps $\tau = 0.0001$, adaptive time steps and large time steps $\tau = 0.01$ (a), and the size of time steps in the adaptive procedure (b)

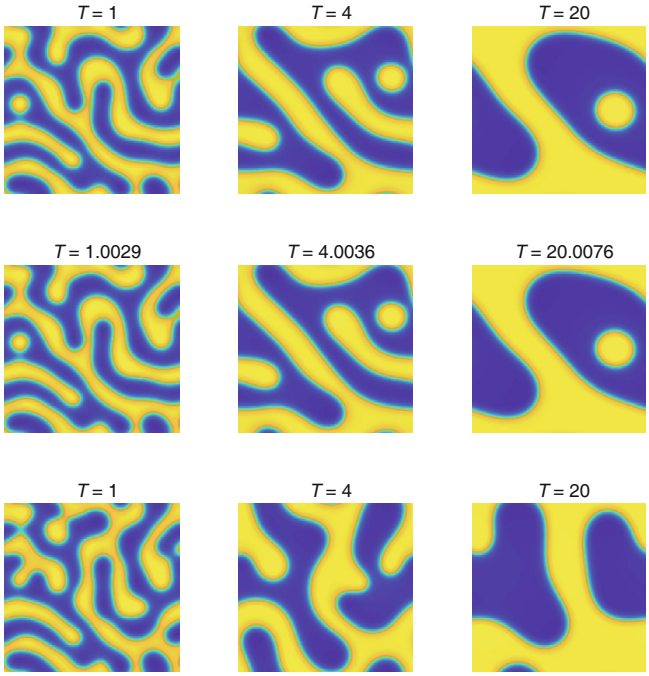

Figure 11 (Color online) Solutions for the Cahn-Hilliard equation using small time steps $\tau = 0.0001$ (first line), adaptive time steps (second line), and large time steps $\tau = 0.01$ (third line)

We plot in Figure 10 the energy curses (a) and the size of adaptive time steps (b). We observe that the solution obtained with $\tau = 10^{-2}$ is not accurate, while the adaptive time-stepping solutions are in excellent agreement with the small time-step solution with $\tau = 10^{-4}$. In addition, except at the initial time period and two other small time intervals where the energy varies drastically, the adaptive time steps basically stay around $\tau = 10^{-2}$. Finally, we plot in Figure 11 snapshots of the phase evolution at different times.

5 Concluding remarks

In this paper, we present a general framework for constructing unconditionally energy-stable ETDRK schemes of arbitrary order for a class of gradient flows and identify a set of conditions that must be satisfied for an ETDRK scheme to be unconditionally energy-stable. In particular, we show that the widely-employed third- and fourth-order ETDRK schemes are not unconditionally energy stable and construct new third-order ETDRK schemes which are unconditionally energy stable.

To the best of our knowledge, this is the first rigorous result on unconditionally energy-stable ETDRK schemes higher than second-order. Potential future extensions include the following:

• Higher than third-order schemes: While we provided a set of conditions that ETDRK schemes need to satisfy in order to be unconditionally energy stable, due to the complexity of these conditions, the existence of higher than third-order ETDRK unconditionally energy stable schemes is still an open question. One possibility is to add one more stage in the RK part which will lead to more free parameters to choose from.

• Other models: We restricted ourselves to a class of gradient flows with Lipschitz nonlinearities. Since the ETDRK schemes are based on Duhamel's principle so that the only error comes from the numerical integration, we expect that the new ETDRK schemes would behave well for other models with even more complicated physical structures, although proving rigorously unconditionally energy stability for more

complicated models would be a challenge.

We are hopeful that our results in this paper can be extended to more general systems and to ETDRK schemes higher than third-order.

Acknowledgements Jie Shen was supported by National Natural Science Foundation of China (Grant No. 12371409). Jiang Yang was supported by National Natural Science Foundation of China (Grant No. 12271240), National Natural Science Foundation of China/Hong Kong Research Grants Council Joint Research Scheme (Grant No. 11961160718), and the Shenzhen Natural Science Fund (Grant No. RCJC20210609103819018).

References

1 Akrivis G, Li B, li D. Energy-decaying extrapolated RK-SAV methods for the Allen-Cahn and Cahn-Hilliard equations. SIAM J Sci Comput, 2019, 41: A3703–A3727
2 Allen S M, Cahn J W. A microscopic theory for antiphase boundary motion and its application to antiphase domain coarsening. Acta Metall, 1979, 27: 1085–1095
3 Cao W, Yang H, Chen W. An exponential time differencing Runge-Kutta method ETDRK32 for phase field models. J Sci Comput, 2024, 99: 6
4 Chen W, Wang X, Yan Y, et al. A second order BDF numerical scheme with variable steps for the Cahn-Hilliard equation. SIAM J Numer Anal, 2019, 57: 495–525
5 Cheng Q, Liu C, Shen J. A new Lagrange multiplier approach for gradient flows. Comput Methods Appl Mech Engrg, 2020, 367: 113070
6 Cheng Q, Shen J. Multiple scalar auxiliary variable (MSAV) approach and its application to the phase-field vesicle membrane model. SIAM J Sci Comput, 2018, 40: A3982–A4006
7 Cox S M, Matthews P C. Exponential time differencing for stiff systems. J Comput Phys, 2002, 176: 430–455
8 Du Q, Ju L, Li X, et al. Maximum principle preserving exponential time differencing schemes for the nonlocal Allen-Cahn equation. SIAM J Numer Anal, 2019, 57: 875–898
9 Du Q, Ju L, Li X, et al. Maximum bound principles for a class of semilinear parabolic equations and exponential time-differencing schemes. SIAM Rev, 2021, 63: 317–359
10 Du Q, Zhu W. Stability analysis and application of the exponential time differencing schemes. J Comput Math, 2004, 22: 200–209
11 Eyre D J. An unconditionally stable one-step scheme for gradient systems. Http://www.math.utah.edu/eyre/research/methods/stable.ps., 1997
12 Feng X, Tang T, Yang J. Long time numerical simulations for phase-field problems using p-adaptive spectral deferred correction methods. SIAM J Sci Comput, 2015, 37: A271–A294
13 Fu Z, Tang T, Yang J. Energy diminishing implicit-explicit Runge-Kutta methods for gradient flows. Math Comp, 2024, 93: 2745–2767
14 Fu Z, Yang J. Energy-decreasing exponential time differencing Runge-Kutta methods for phase-field models. J Comput Phys, 2022, 454: 110943
15 Gomez H, Hughes T J R. Provably unconditionally stable, second-order time-accurate, mixed variational methods for phase-field models. J Comput Phys, 2011, 230: 5310–5327
16 He Y, Liu Y, Tang T. On large time-stepping methods for the Cahn-Hilliard equation. Appl Numer Math, 2006, 57: 616–628
17 Hochbruck M, Ostermann A. Explicit exponential Runge-Kutta methods for semilinear parabolic problems. SIAM J Numer Anal, 2006, 43: 1069–1090
18 Hochbruck M, Ostermann A. Exponential integrators. Acta Numer, 2010, 19: 209–286
19 Hou D, Qiao Z. An implicit-explicit second-order BDF numerical scheme with variable steps for gradient flows. J Sci Comput, 2023, 94: 39
20 Huang F, Shen J. A new class of implicit-explicit BDFk SAV schemes for general dissipative systems and their error analysis. Comput Methods Appl Mech Engrg, 2022, 392: 114718
21 Ju L, Li X, Qiao Z. Generalized SAV-exponential integrator schemes for Allen-Cahn type gradient flows. SIAM J Numer Anal, 2022, 60: 1905–1931
22 Krogstad S. Generalized integrating factor methods for stiff PDEs. J Comput Phys, 2005, 203: 72–88
23 Li B O, Liu J G. Thin film epitaxy with or without slope selection. European J Appl Math, 2003, 14: 713–743
24 Li D, Qiao Z. On second order semi-implicit Fourier spectral methods for 2D Cahn-Hilliard equations. J Sci Comput, 2017, 70: 301–341
25 Li D, Qiao Z, Tang T. Characterizing the stabilization size for semi-implicit Fourier-spectral method to phase field equations. SIAM J Numer Anal, 2016, 54: 1653–1681

26 Li X, Qiao Z, Wang C. Convergence analysis for a stabilized linear semi-implicit numerical scheme for the nonlocal Cahn-Hilliard equation. Math Comp, 2021, 90: 171–188

27 Li X, Shen J. Stability and error estimates of the SAV Fourier-spectral method for the phase field crystal equation. Adv Comput Math, 2020, 46: 48

28 Li X, Shen J. Efficient linear and unconditionally energy stable schemes for the modified phase field crystal equation. Sci China Math, 2022, 65: 2201–2218

29 Luo F, Tang T, Xie H. Parameter-free time adaptivity based on energy evolution for the Cahn-Hilliard equation. Commun Comput Phys, 2016, 19: 1542–1563

30 Shen J, Tang T, Yang J. On the maximum principle preserving schemes for the generalized Allen-Cahn equation. Commun Math Sci, 2016, 14: 1517–1534

31 Shen J, Wang C, Wang X, et al. Second-order convex splitting schemes for gradient flows with Ehrlich-Schwoebel type energy: Application to thin film epitaxy. SIAM J Numer Anal, 2012, 50: 105–125

32 Shen J, Xu J, Yang J. The scalar auxiliary variable (SAV) approach for gradient flows. J Comput Phys, 2018, 353: 407–416

33 Shen J, Xu J, Yang J. A new class of efficient and robust energy stable schemes for gradient flows. SIAM Rev, 2019, 61: 474–506

34 Shen J, Yang X. Numerical approximations of Allen-Cahn and Cahn-Hilliard equations. Discrete Contin Dyn Syst, 2010, 28: 1669–1691

35 Shin J, Lee H G, Lee J Y. Convex splitting Runge-Kutta methods for phase-field models. Comput Math Appl, 2017, 73: 2388–2403

36 Tang T. Revisit of semi-implicit schemes for phase-field equations. Anal Theory Appl, 2020, 36: 235–242

37 Tang T, Wu X, Yang J. Arbitrarily high order and fully discrete extrapolated RK-SAV/DG schemes for phase-field gradient flows. J Sci Comput, 2022, 93: 38

38 Tang T, Yang J. Implicit-explicit scheme for the Allen-Cahn equation preserves the maximum principle. J Comput Math, 2016, 34: 451–461

39 Xu C, Tang T. Stability analysis of large time-stepping methods for epitaxial growth models. SIAM J Numer Anal, 2006, 44: 1759–1779

40 Yang X. Linear, first and second-order, unconditionally energy stable numerical schemes for the phase field model of homopolymer blends. J Comput Phys, 2016, 327: 294–316

41 Yang X, Zhao J, Wang Q, et al. Numerical approximations for a three-component Cahn-Hilliard phase-field model based on the invariant energy quadratization method. Math Models Methods Appl Sci, 2017, 27: 1993–2030

42 Zhang Z, Qiao Z. An adaptive time-stepping strategy for the Cahn-Hilliard equation. Commun Comput Phys, 2012, 11: 1261–1278